

pubs.acs.org/journal/apchd5 Article

# Compact Stereo Waveguide Display Based on a Unidirectional Polarization-Multiplexed Metagrating In-Coupler

Zeyang Liu, Cheng Zhang,\* Wenqi Zhu, Zhanhua Huang, Henri J. Lezec, Amit Agrawal, and L. Jay Guo\*



Cite This: ACS Photonics 2021, 8, 1112-1119



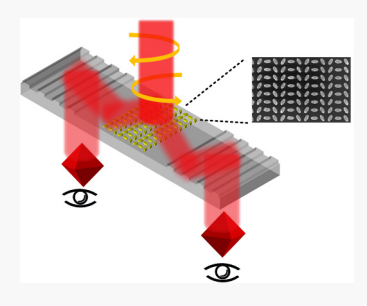
**ACCESS** 

Metrics & More



Supporting Information

ABSTRACT: Three-dimensional (3D) vision in augmented reality (AR) displays can enable highly immersive and realistic viewer experience, hence, attracts much attention. Most current approaches create 3D vision by projecting stereoscopic images to different eyes using two separate projection systems, which are inevitably bulky for wearable devices. Here, we propose a compact stereo waveguide AR display system using a single piece of thin flat glass integrated with a polarization-multiplexed metagrating in-coupler and two diffractive grating out-couplers. Incident light of opposite circular polarization states carrying stereoscopic images are first steered by the metagrating in-coupler to opposite propagation directions in the flat glass waveguide, subsequently extracted by the diffractive grating out-couplers, and finally received by different eyes, forming 3D stereo vision. Experimentally, we fabricated a display prototype and



demonstrated independent projection of two polarization-multiplexed stereoscopic images. This work paves a novel path toward the implementation of high-performance stereo displays with compact size, lightweight, and multicolor compatibility.

KEYWORDS: waveguide display, stereo display, augmented reality display, metasurface, unidirectional coupling

A ugmented reality (AR) display can superimpose virtual images over a real-world scene and enables the user to observe both simultaneously. As it may lead to a new paradigm in many areas, including navigation, education, surgery, and entertainment, the research of AR display devices, namely, near-to-eye see-through displays, is booming and has attracted considerable attention over the past decade. Various approaches such as freeform optical prisms, projection systems, retina scanning, reflective systems, hybrid reflective-refractive systems, and optical waveguides have been proposed. Related commercial products have also been released by some major corporations, such as Sony, Google, Microsoft, and so on.

Among these various approaches, optical waveguide technology is considered as the most promising means toward realizing lightweight and compact devices of high performance; thus, it enjoys rapid development. A transparent optical waveguide acts as an off-axis imaging system that projects images to human eye(s) without blocking the ambient scene. For AR display, a three-dimensional (3D) vision is highly desirable because it can provide an immersive and realistic experience for the viewer. Although various approaches have been proposed to realize 3D AR display, 13-17 this functionality has been a challenge for optical waveguide-based approaches. One common method to address the aforementioned limitation utilizes holographic gratings as couplers to reconstruct 3D objects, but it suffers from low image quality and small field of view (FOV). 18,19 Stereoscopy provides another approach to create 3D depth perception, which arises from the given two-dimensional images representing two perspectives of the same object that both eyes naturally receive in binocular vision. The stereo waveguide display is usually realized by using two waveguides as subsystems to respectively project stereoscopic images from two images sources to different eyes, which inevitably results in a bulky volume and increased difficulty for integration. In recent years, metasurfaces, which are composed of two-dimensional metallic or dielectric nanostructures of subwavelength scale, have received tremendous attention. Various planar optical devices such as filters, <sup>20,21</sup> lenses, <sup>22–25</sup> polarizers, <sup>26,27</sup> and absorbers <sup>28,29</sup> have been implemented by diverse reflective or transmissive metasurfaces, featuring high optical performance, as well as an ultracompact footprint. Apart from engineering light in free space, metasurfaces have also demonstrated the ability to manipulate guided light, primarily focusing in the near-infrared spectral range for communication applications.  $^{30-33}$  Compared to conventional couplers such as prisms and gratings, metasurface couplers offer a unique feature of unidirectional in-coupling that can be controlled by the polarization state of incident light.

Here, targeting at visible light, we design a geometric-phase-based metagrating paired with two diffractive gratings on a thin fused-silica substrate as a compact platform to realize polarization-multiplexed in-coupling for stereo waveguide

Received: December 11, 2020 Published: March 22, 2021





display. Incident circularly polarized light (CPL) illuminating the metagrating is deflected into the underlying substrate, and satisfies the total internal reflection (TIR) condition to propagate inside this flat waveguide. The deflection angle is determined by the phase gradient imposed by the metagrating, which is opposite for CPL of opposite handedness. Therefore, incident light with opposite handedness bearing two stereoscopic images can be in-coupled along opposite directions inside the waveguide and finally out-coupled to different eyes, generating 3D vision for the viewer. As a prototype demonstration, unidirectional in-coupling with a high contrast ratio for opposite CPL incidence is achieved by the metagrating and independent projection of two stereoscopic images multiplexed by polarization is demonstrated.

#### DESIGN OF THE METAGRATING IN-COUPLER

A schematic layout of the proposed stereo waveguide display based on unidirectional polarization-multiplexed in-coupling is shown in Figure 1. The system comprises of a microdisplay, a

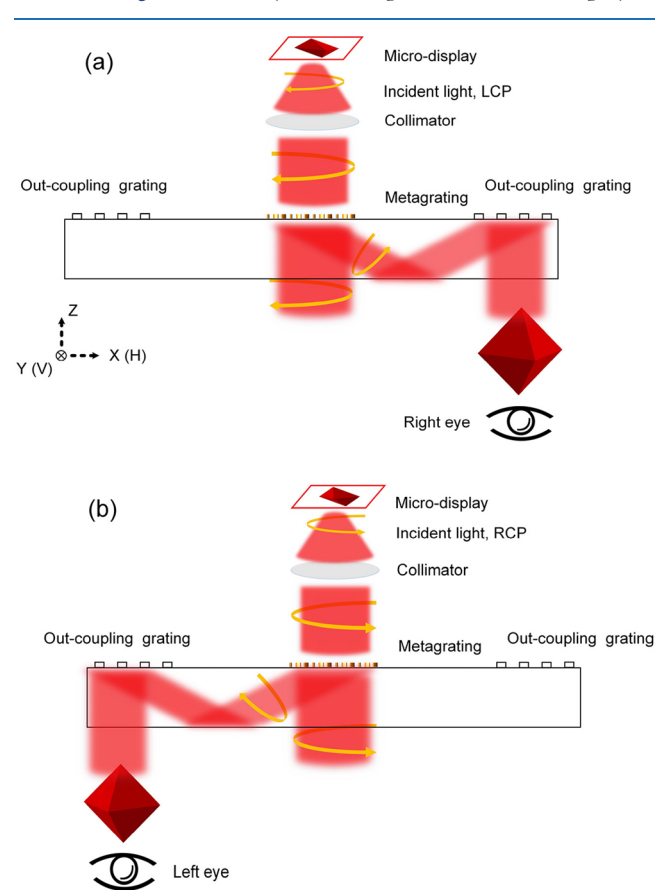


**Figure 1.** Schematics illustrating the stereo waveguide display based on unidirectional polarization-multiplexed in-coupling. When the handedness of incident CPL is flipped, as shown by (a) and (b), incoupling direction becomes opposite and the stereoscopic images can be delivered to different eyes. H: horizontal direction; V: vertical direction.

collimator, and a glass waveguide that is integrated with a metagrating in-coupler and two surface-relief grating out-couplers. The metagrating is designed based on geometric phase, which can lead to opposite deflection directions for CPL with opposite handedness. Image bearing light in circular polarization states from the microdisplay is first collimated and

then deflected by the metagrating following the phase gradient direction. Deflected light toward the bottom surface of the waveguide has an angle greater than the critical angle of TIR, ensuring that the light stays confined as it propagates within the waveguide. At the end of the waveguide, the out-coupling grating diffracts the guided light, extracting it from the waveguide and projecting it onto the human eye. The periods of the in- and out-couplers are designed to be the same to guarantee no distortion of the projected images after propagation along the folded light paths inside the waveguide. When the circular polarization of incident light is switched to the opposite state, so does the deflection as well as the incoupling direction. Using this approach, incident light in opposite circular polarizations carrying two stereoscopic images can be received separately by the two eyes to create 3D vision.

The metagrating in-coupler consists of anisotropic Au nanobars that have same size but different rotational orientations to produce the desired geometric phase gradient. They can convert the incident CPL to its cross-polarization and simultaneously induce a phase shift that is twice the orientation angle of the nanobars. By arranging nanobars with linearly changing orientation angles, transmitted light in cross-polarization can be deflected, which is commonly interpreted as anomalous refraction. For incident CPL with opposite handedness, the induced geometric phase acquires an opposite sign, and therefore the transmitted light is deflected to the opposite direction. When the phase gradient is steep enough, the deflection angle satisfies the TIR condition, thereby leading to the required polarization-multiplexed incoupling. In a conical geometry, the in-coupling condition can be expressed by eqs 1 and 2:

$$n_1 \sin \theta_{\rm d} \sin \varphi_{\rm d} = n_0 \sin \theta_{\rm i} \sin \varphi_{\rm i} \tag{1}$$

$$n_1 > n_1 \sin \theta_{\rm d} \cos \varphi_{\rm d} = n_0 \sin \theta_{\rm i} \cos \varphi_{\rm i} + \frac{\lambda}{2\pi} \frac{\mathrm{d}\phi}{\mathrm{d}x}$$
  
=  $n_0 \sin \theta_{\rm i} \cos \varphi_{\rm i} + \frac{\lambda}{T} > 1$  (2)

where  $\lambda$  is the free-space wavelength of the incoming light; T is the period of the metagrating;  $d\phi/dx$  denotes the phase gradient, which equals  $2\pi/T$  for the designed metagrating.  $n_0$ and  $n_1$  are the refractive indices of air and the waveguide material, respectively;  $\theta_i$  and  $\theta_d$  are the incident and deflection polar angles, respectively, defined in the plane of incidence, as shown in Figure 2.  $\varphi_i$  and  $\varphi_d$  are the incident and deflection azimuthal angles, respectively, defined along the plane of the metagrating (Figure.2). The right-hand-side inequality of eq 2 decides the upper limit of the period in order to satisfy the TIR condition, while the left-hand-side relation gives the lower limit to ensure the existence of deflection (anomalous refraction). According to the in-coupling condition of eq 2, the phase gradient of the metagrating determines the deflection angle, therefore, it also determines the angular range of the incident light that can be coupled into the waveguide, namely the FOV, which is related to the size of the projected image. The horizontal and vertical FOVs are the components of the incident angle  $\theta_i$  on the X-Z and Y-Z plane, respectively. They are denoted by  $\theta_H$  and  $\theta_V$  in the inset of Figure 2 and can be described by eqs 3 and 4. Targeting operation with red light  $(\lambda = 635 \text{ nm})$ , the period of the metagrating is optimized to be 555 nm such that a maximum diagonal FOV of  $20^{\circ}$  ( $16^{\circ}H \times$ 12°V) can be realized.

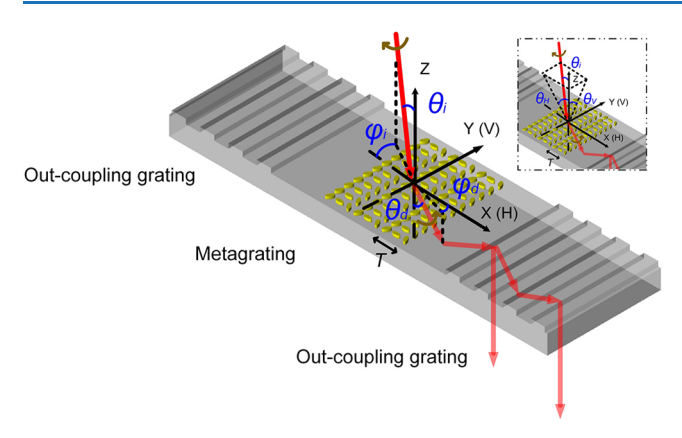


**Figure 2.** Schematic showing the in-coupling and out-coupling of the waveguide system.  $\theta_H$  and  $\theta_V$  shown in the inset are the components of the incident angle  $\theta_i$  on the X-Z and Y-Z planes, respectively, representing the horizontal and vertical FOV, respectively.

$$\theta_{H} = \arctan(\tan(\theta_{i}) \cos(\varphi_{i})) \tag{3}$$

$$\theta_V = \arctan(\tan(\theta_i) \sin(\varphi_i))$$
 (4)

The structure of the metagrating is shown in Figure 3a. Each period contains three equally spaced Au elliptical nanobars, with orientation angles of  $-60^{\circ}$ ,  $0^{\circ}$ , and  $60^{\circ}$ , respectively, to cover a phase shift range of  $2\pi$ . The long axis of each nanobar is 160 nm and the short axis is 70 nm. The simulated wavefronts of the transmitted light for normal incidence are shown in Figure 3b–d. Light in co-polarization state remains in the same propagation direction, but cross-polarized light is

deflected with an angle of 51.6° inside the substrate and undergoes TIRs at the fused-silica/air interface. The deflection direction becomes opposite when the handedness of the incident CPL light is flipped. For the metagrating, every three elliptic nanobars constitute a period. From the perspective of periodic diffraction, one can treat the anomalous refraction and normal refraction as the +1st order and the 0th order diffraction, respectively, while the -1st order is strongly suppressed. The in-coupling unidirectionality  $\gamma$  is defined as the intensity contrast ratio between the +1st order and -1st order  $(T_1/T_{-1})$ , which ranges from 6.2 to 14.1 across the horizontal FOV, as shown by Figure 3e. Figure 3f and g present the light propagation paths by TIRs inside a fusedsilica waveguide for left circularly polarized (LCP) and right circularly polarized (RCP) incidence, respectively, clearly showing opposite deflection and unidirectional in-coupling. The thickness of the waveguide is set to 10  $\mu$ m for ease of simulation.

## RAY-TRACING SIMULATION OF THE WAVEGUIDE SYSTEM

To further verify the unidirectional coupling and the FOV achievable in a waveguide system, ray-tracing simulation is implemented. In simulation, the period of the diffractive grating out-coupler is set to 555 nm as well, with an out-coupling efficiency of 10% in each diffraction. The size of the waveguide system is shown in Figure 4, which is set after taking into account the actual size that is needed for a wearable bonocular AR device. The two eye boxes are  $10 \text{ mm} \times 5 \text{ mm}$  at an eye relief of 20 mm and their distance is 60 mm. The

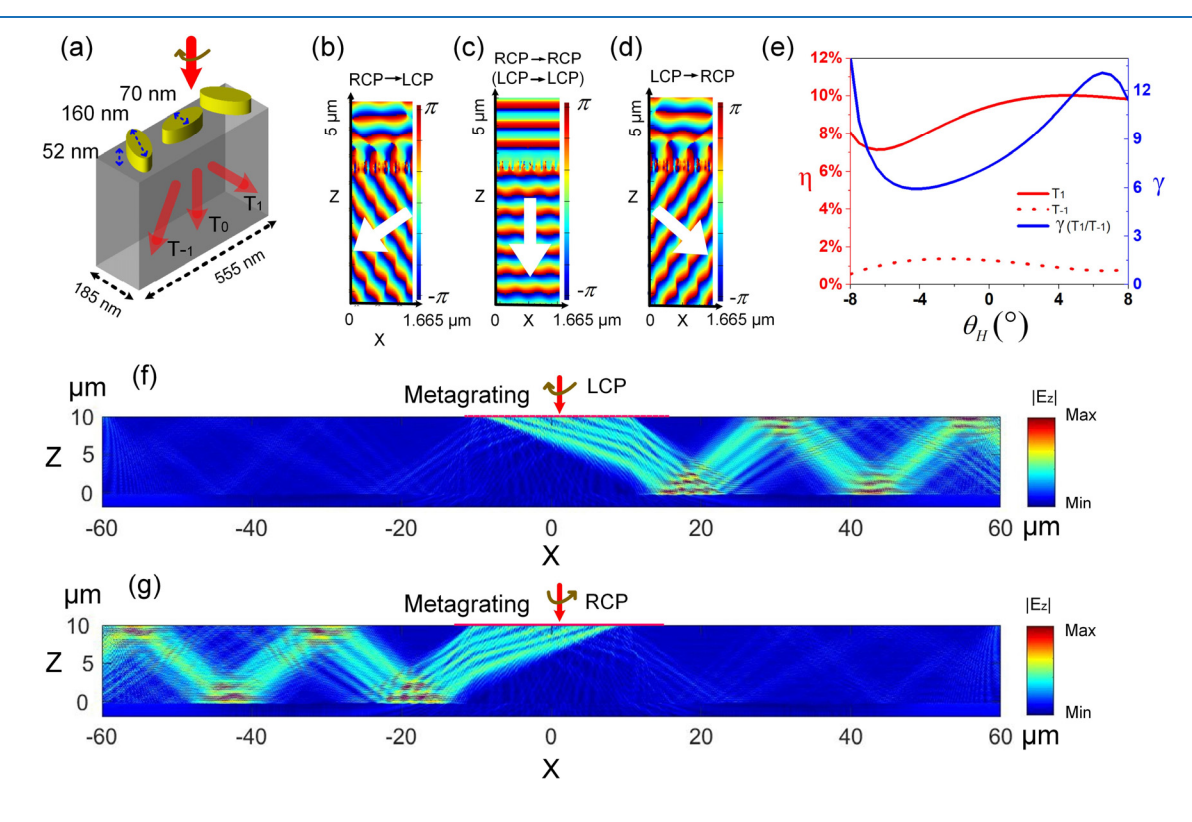


Figure 3. (a) Structure of the metagrating in a single period consisting of three Au nanobars of different orientations. (b)–(d) Simulated wavefronts of the transmitted light in cross-polarization and in co-polarization states. (b) and (d) indicate that flipping the handedness of incident light leads to opposite deflections. (e) Simulated diffraction efficiency  $\eta$  of the two first orders and their intensity contrast ratio (unidirectionality)  $\gamma$  across the horizontal FOV. (f, g) Distributions of  $|E_z|$  inside a 10  $\mu$ m thick fused-silica waveguide for LCP/RCP incidence. Coupled light propagates inside the waveguide by TIR along positive/negative direction of the X-axis, respectively. The red line indicates the metagrating.

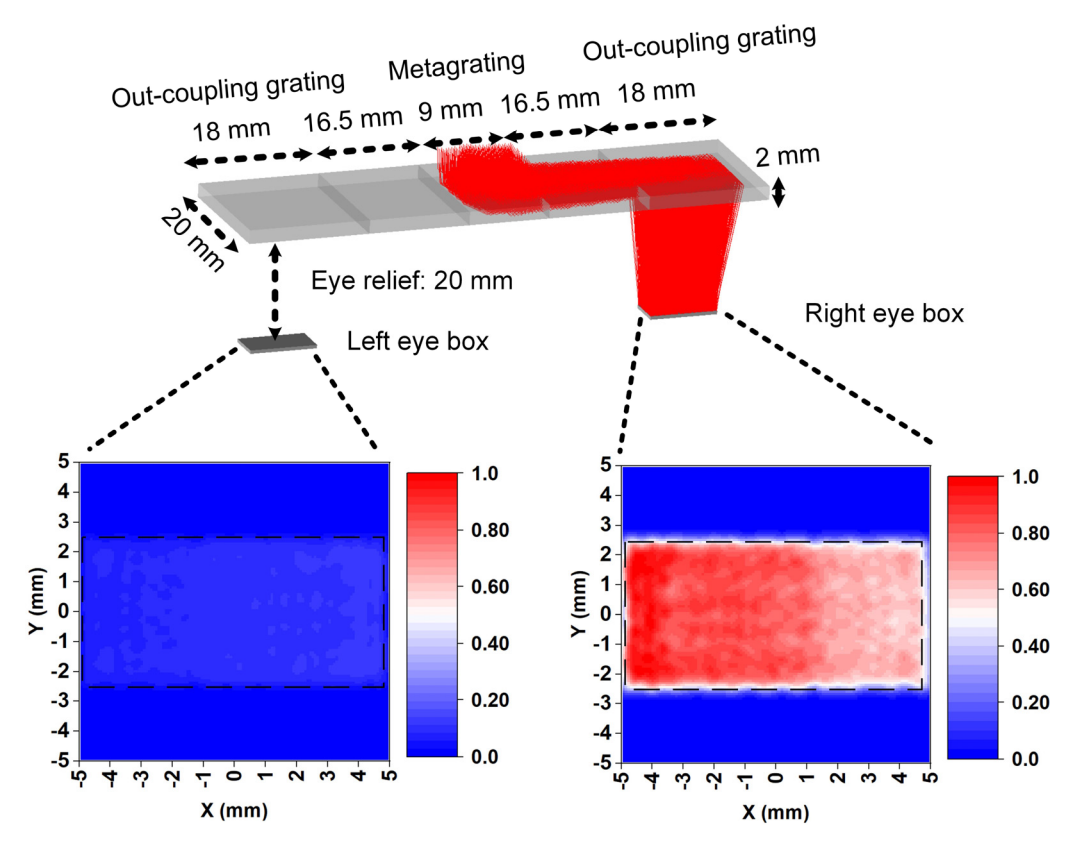


Figure 4. Ray-tracing simulation of the stereo waveguide display. The luminance distributions are normalized to the maximum value on the right eye box. The maximum of the normalized luminance on left eye box is 0.13.

incident angle varies from  $-8^{\circ}$  to  $8^{\circ}$  horizontally and from  $-6^{\circ}$ to  $6^{\circ}$  vertically, in accordance with the maximum achievable FOV. Taking LCP incidence as an example, 1200 rays are input into the waveguide system and the normalized luminance distributions over the two eye boxes are presented in Figure 4. The horizontally gradual decrease of normalized luminance intensity is due to the repeated out-coupling diffraction of the guided light. As shown, most of the in-coupled light propagates to the right side of the waveguide. Compared to the right eye box, the luminance on the left eye box is significantly lower with a maximum value of 0.13, corresponding to a contrast ratio greater than 7, which agrees well with the in-coupling unidirectionality of the metagrating. The results indicate that the impact of LCP incident light on the left exit pupil is negligible, which enables independent projection of two polarization-multiplexed images to different eyes. As the geometric phase has broadband property and light in the 0th order transmitting through the waveguide can preserve handedness upon transmission, this design can be expanded to use a stack of multiple layers of waveguides to display multiple colors. We demonstrate unidirectional in-coupling of light in three colors using two layers of waveguides by simulation, as shown in the Supporting Information.

# **EXPERIMENTS AND RESULTS**

For a proof-of-principle experiment, we fabricated the designed metagrating with a size of 0.7 mm  $(X) \times 1.4$  mm (Y) on a 2 mm thick fused-silica waveguide. A representative scanning electron microscope (SEM) image of the metagrating is shown in Figure 5a. To characterize the unidirectional in-coupling of the metagrating, in-coupling efficiency and unidirectional coupling ratio are measured. Circularly polarized light is

incident on the metagrating, and a portion of it is in-coupled into the fused-silica waveguide. The in-coupled light is extracted by using a prism and its intensity is measured, as shown in Figure 5b. When the incident angle changes across the FOV, the in-coupling efficiency is approximately 8%. To measure the in-coupling unidirectionality, we flipped the handedness of incident light and observed high intensity contrast of the out-coupled light, with a ratio of approximately 7.5. The experimental results agree well with the simulation in Figure 3e. It is worth noting that the relatively low coupling efficiency as well as the in-coupling unidirectionality can be significantly improved by using high refractive index dielectric material for the metagrating, such as Si, to enhance the interaction between the nanostructures and incident light.<sup>37,38</sup> In order to visualize the impact of handedness of incident light on the projected image, we fabricated a surface-relief diffractive grating on the waveguide, using nanoimprint lithography, 39,40 as the out-coupler to extract the in-coupled light. Corresponding SEM image of the imprinted grating is shown in Figure 5c. The out-coupling grating has a size of 2 cm  $(X) \times 1$  cm (Y)and it is made of transparent UV-curable polyurethane acrylate (PUA) resin. We made an M-shaped pattern (width = 400  $\mu$ m) on a photomask and illuminated red light on it as the image source. The experimental setup is shown in Figure 5d. For LCP incidence, a bright projected image "M" can be clearly seen overlaying on an ambient scene; when the incident light polarization is changed to RCP, the pattern became considerably dim and neglectable, as shown in Figure 5e,f. To further demonstrate the stereo display enabled by the metagrating design, we made two photomasks with two stereoscopic patterns (width = 200  $\mu$ m) representing two perspective views of an octahedron, as depict in Figure 6a.

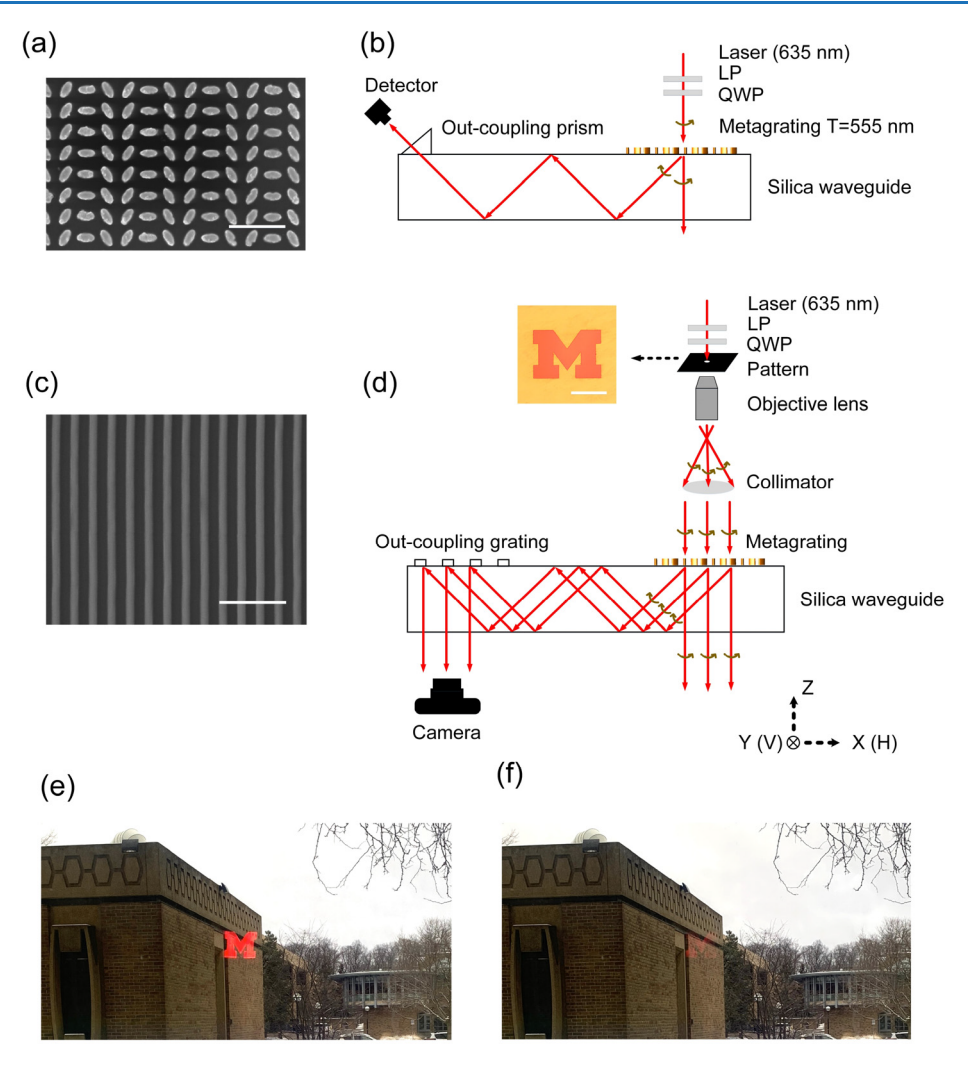


Figure 5. (a) SEM image of the metagrating (scale bar: 500 nm). (b) Experimental setup for the measurement of in-coupling efficiency and incoupling unidirectionality. (c) SEM image of the imprinted out-coupling grating (scale bar:  $2 \mu m$ ). (d) Experimental setup to show the impact of handedness of incident light on the projected image. The objective lens ( $10 \times magnification$ , NA = 0.25) is used to magnify the pattern. Inset is the optical micrograph of the M-shaped pattern on the photomask (scale bar:  $200 \mu m$ ). (e, f) The projected pattern overlapped on an ambient scene for RCP and LCP incidence, respectively. QWP: quarter wave plate; LP: linear polarizer.

Out-coupling gratings are imprinted on both ends of the waveguide. Two beams in orthogonal linear polarization states are illuminated on the two masks to bear the image information. After collimation, the two beams are converted to LCP and RCP, respectively, by a quarter wave plate and finally imaged onto different cameras, which mimic the left and right eyes. The experimental setup is shown in Figure 6b, and the experimental results are presented in Figure 6c,d. As can be seen, the two stereoscopic patterns can be received independently with high fidelity and negligible crosstalk, which verifies the feasibility of this design. In actual display devices, stereoscopic images in different polarizations can be provided by a microdisplay combined with an electronic polarization modulator to change the polarization of emitted light along with the switching of stereoscopic images in real time, such that 3D video images can be displayed by this device.

#### SUMMARY

In this paper, we propose and experimentally demonstrate a stereo waveguide display that employs a metagrating in-coupler paired with two diffractive grating out-couplers. The metagrating is designed based on geometric phase and can impose a handedness-dependent phase gradient that is steep enough to satisfy the in-coupling condition. Stereoscopic images carried by incident light with opposite handednesses can be coupled into the waveguide along opposite directions and delivered to different eyes, generating 3D vision for the viewer. Although the prototype only demonstrates monochromatic images, the underlying design is compatible with stacking multiple layers of waveguides for multicolor display. This metagrating for polarization-multiplexed unidirectional in-coupling can simplify the configuration of stereo waveguide displays by involving less optical elements, making the system more compact, lighter weight, and easier for integration. This design could find promising applications in various mixed reality display devices as well as in integrated optics.

# METHODS

The metagrating was fabricated on a 500  $\mu$ m thick fused-silica substrate using electron beam lithography followed by metal lift-off. Two 100 nm thick layers of poly methyl methacrylate (PMMA) electron beam resist of different molecular weights (PMMA 495K and 950 K) were consecutively spin-coated

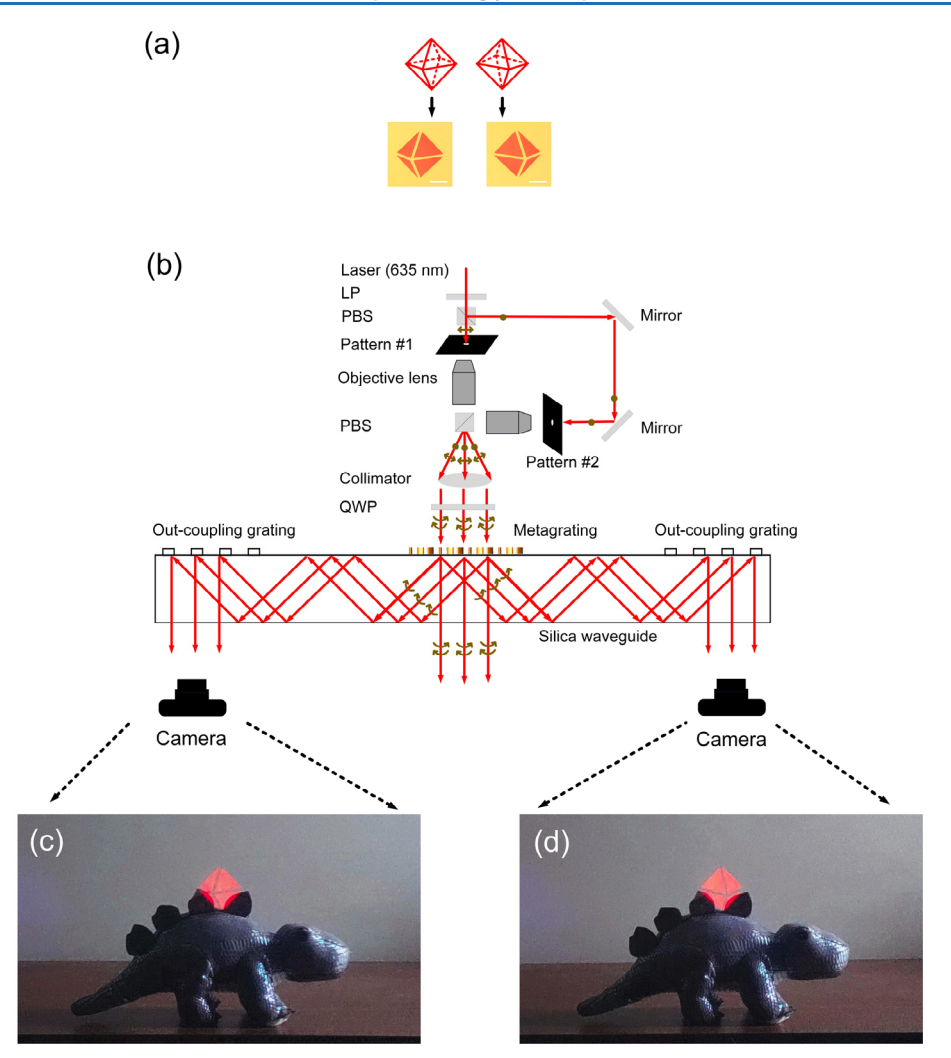


Figure 6. (a) Two stereoscopic patterns representing two perspectives of different eyes of an octahedron and the corresponding optical micrographs of the patterns on the photomasks. Scale bar:  $100 \, \mu \text{m}$ . (b) Experimental setup to demonstrate the stereo waveguide display based on unidirectional polarization-multiplexed in-coupling enabled by the metagrating. (c, d) Two stereoscopic virtual images overlapped on an ambient scene are received by the two cameras on the left and the right sides, respectively. PBS: polarization beam splitter.

onto the fused-silica substrate, followed by thermal evaporation of a 20 nm thick Al charge-dissipation layer. A 100 keV electron beam system was used to expose the metagrating pattern, followed by Al removal with tetramethylammonium hydroxide and PMMA development with methyl isobutyl ketone. The developed pattern in the PMMA bilayer was used to lift off an electron-beam-evaporated 52 nm thick Au layer (with 5 nm thick Ti adhesion layer). The fused-silica substrate with metagrating was then adhered onto a 1.5 mm thick flat fused-silica to constitute a 2 mm thick waveguide. The outcoupling diffractive gratings were imprinted using a Si mold. The mold's surface was treated by gas-phase deposition of tridecafluoroctyltrichlorosilane for antisticking in advance. A total of 5  $\mu$ L of polyurethane acrylate (PUA) resin was dropcast on the fused-silica substrate and then covered by the mold. After aligning the mold to the metagrating, UV light from a spot UV curing system ( $\lambda = 365$  nm, 200 W) was illuminated on the PUA resin for 3 min to fully cure it, during which slight pressure was applied on the mold for conformal contact. Thereafter, the mold was manually separated from the substrate, leaving the imprinted grating structures on it.

## ASSOCIATED CONTENT

#### Supporting Information

The Supporting Information is available free of charge at https://pubs.acs.org/doi/10.1021/acsphotonics.0c01885.

Stacking two layers of waveguides for multicolor stereo display (PDF)

#### AUTHOR INFORMATION

#### **Corresponding Authors**

Cheng Zhang — School of Optical and Electronic Information and Wuhan National Laboratory for Optoelectronics, Huazhong University of Science and Technology, Wuhan 430074, China; orcid.org/0000-0002-9739-3511; Email: cheng.zhang@hust.edu.cn

L. Jay Guo – Department of Electrical Engineering and Computer Science, University of Michigan, Ann Arbor, Michigan 48109, United States; orcid.org/0000-0002-0347-6309; Email: guo@umich.edu

#### **Authors**

Zeyang Liu – Department of Electrical Engineering and Computer Science, University of Michigan, Ann Arbor,

**ACS Photonics** Article pubs.acs.org/journal/apchd5

- Michigan 48109, United States; Key Laboratory of Optoelectronics Information Technology, Ministry of Education, Tianjin University, Tianjin 300072, China; orcid.org/0000-0002-1647-2892
- Wengi Zhu Physical Measurement Laboratory, National Institute of Standards and Technology, Gaithersburg, Maryland 20899, United States; Maryland NanoCenter, University of Maryland, Maryland 20742, United States; orcid.org/0000-0001-7832-189X
- Zhanhua Huang Key Laboratory of Optoelectronics Information Technology, Ministry of Education, Tianjin University, Tianjin 300072, China
- Henri I. Lezec Physical Measurement Laboratory, National Institute of Standards and Technology, Gaithersburg, Maryland 20899, United States
- Amit Agrawal Physical Measurement Laboratory, National Institute of Standards and Technology, Gaithersburg, Maryland 20899, United States; Maryland NanoCenter, University of Maryland, Maryland 20742, United States; orcid.org/0000-0002-9619-7623

Complete contact information is available at: https://pubs.acs.org/10.1021/acsphotonics.0c01885

#### **Notes**

The authors declare no competing financial interest.

#### ACKNOWLEDGMENTS

This work is supported in part by National Science Foundation (CMMI-1635636). Z.L. acknowledges the financial support from China Scholarship Council (CSC). Z.L. and Z.H. acknowledge support from National Natural Science Foundation of China (61475113). C.Z. acknowledges the start-up funding from the Huazhong University of Science and Technology. W.Z. and A.A. acknowledge support under the Cooperative Research Agreement between the University of Maryland and the National Institute of Standards and Technology Physical Measurement Laboratory, Award 70NANB14H209, through the University of Maryland. Certain commercial equipment, instruments, materials, or software are identified in this paper to foster understanding. Such identification does not imply recommendation or endorsement by the National Institute of Standards and Technology nor does it imply that the materials or equipment identified are necessarily the best available for the purpose.

## REFERENCES

- (1) Yamazaki, S.; Inoguchi, K.; Saito, Y.; Morishima, H.; Taniguchi, N. Thin, wide field-of -view HMD with free-form-surface prism and applications. Proc. SPIE 1999, 3639, 453-462.
- (2) Cheng, D.; Wang, Y.; Hua, H.; Talha, M. M. Design of an optical see-through head-mounted display with a low f-number and large field of view using a freeform prism. Appl. Opt. 2009, 48, 2655-2668.
- (3) Hua, H.; Girardot, A.; Gao, C.; Rolland, J. P. Engineering of head-mounted projective displays. Appl. Opt. 2000, 39, 3814-3824.
- (4) Martins, R.; Shaoulov, V.; Ha, Y.; Rolland, J. P. A mobile headworn projection display. Opt. Express 2007, 15, 14530-14538.
- (5) Bayer, M. M. Retinal scanning display: a novel HMD approach for Army aviation. Proc. SPIE 2002, 4711, 202.
- (6) Bauer, A.; Rolland, J. P. Visual space assessment of two allreflective, freeform, optical see-through headworn displays. Opt. Express 2014, 22, 13155-13163.
- (7) Yang, J.; Liu, W.; Lv, W.; Zhang, D.; He, F.; Wei, Z.; Kang, Y. Method of achieving a wide field-of-view head-mounted display with small distortion. Opt. Lett. 2013, 38, 2035-2037.

- (8) Amitai, Y. A two-dimensional aperture expander for ultracompact, high-performance head-worn displays. Dig. Tech. Pap. - Soc. Inf. Disp. Int. Symp. 2005, 36, 360-363.
- (9) Cheng, D.; Wang, Y.; Xu, C.; Song, W.; Jin, G. Design of an ultra-thin near-eye display with geometrical waveguide and freeform optics. Opt. Express 2014, 22, 20705-20719.
- (10) Levola, T. Diffractive optics for virtual reality display. J. Soc. Inf. Disp. 2006, 14, 467-475.
- (11) Mukawa, H.; Akutsu, K.; Matsumura, I.; Nakano, S.; Yoshida, T.; Kuwahara, M.; Aiki, K.; Ogawa, M. A full color eyewear display using holographic planar waveguides. Dig. Tech. Pap. - Soc. Inf. Disp. Int. Symp. 2008, 39, 89-92.
- (12) Liu, Z.; Pang, Y.; Pan, C.; Huang, Z. Design of a uniformillumination binocular waveguide display with diffraction gratings and freeform optics. Opt. Express 2017, 25, 30720-30731.
- (13) Huang, H.; Hua, H. High-performance integral-imaging-based light field augmented reality display using freeform optics. Opt. Express 2018, 26, 17578-17590.
- (14) Zhang, Z.; Liu, J.; Gao, Q.; Duan, X.; Shi, X. A full-color compact 3D see-through near-eye display system based on complex amplitude modulation. Opt. Express 2019, 27, 7023-7035.
- (15) Shen, X.; Javidi, B. Large depth of focus dynamic micro integral imaging for optical see-through augmented reality display using a focus-tunable lens. Appl. Opt. 2018, 57, B184-B189.
- (16) Wang, J.; Xiao, X.; Hua, H.; Javidi, B. Augmented reality 3D displays with micro integral imaging. J. Disp. Technol. 2015, 11, 889-893.
- (17) He, Z.; Sui, X.; Jin, G.; Cao, L. Progress in virtual reality and augmented reality based on holographic display. Appl. Opt. 2019, 58,
- (18) Darkhanbaatara, N.; Shin, C.-W.; Erdenebat, M.-U.; Lee, K.-Y.; Kim, N. Holographic waveguide-type three-dimensional augmentedreality display using the holographic optical element-mirror array. Proc. SPIE 2019, 10942, 1094216.
- (19) Jolly, S.; Savidis, N.; Datta, B.; Bove, V. M.; Smalley, D. Progress in off-plane computer-generated waveguide holography for near-to-eye 3D display. Proc. SPIE 2016, 9771, 97710L.
- (20) Cheng, F.; Gao, J.; Luk, T. S.; Yang, X. Structural color printing based on plasmonic metasurfaces of perfect light absorption. Sci. Rep. 2015, 5, 11045.
- (21) Proust, J.; Bedu, F.; Gallas, B.; Ozerov, I.; Bonod, N. Alldielectric colored metasurfaces with silicon mie resonators. ACS Nano **2016**, 10, 7761-7767.
- (22) Khorasaninejad, M.; Chen, W. T.; Devlin, R. C.; Oh, J.; Zhu, A. Y.; Capasso, F. Metalenses at visible wavelengths: Diffraction-limited focusing and subwavelength resolution imaging. Science 2016, 352, 1190-1194.
- (23) Khorasaninejad, M.; Capasso, F. Metalenses: Versatile multifunctional photonic components. Science 2017, 358 (6367),
- (24) Zhang, C.; Divitt, S.; Fan, Q.; Zhu, W.; Agrawal, A.; Lu, Y.; Xu, T.; Lezec, H. J. Low-loss metasurface optics down to the deep ultraviolet region. Light: Sci. Appl. 2020, 9, 55.
- (25) Dai, W.; Wang, Y.; Li, R.; Fan, Y.; Qu, G.; Wu, Y.; Song, Q.; Han, J.; Xiao, S. Achieving circularly polarized surface emitting perovskite microlasers with all-dielectric metasurfaces. ACS Nano **2020**, 14, 17063-17070.
- (26) Zhang, C.; Pfeiffer, C.; Jang, T.; Ray, V.; Junda, M.; Uprety, P.; Podraza, N.; Grbic, A.; Guo, L. J. Breaking Malus' law: highly efficient, broadband, and angular robust asymmetric light transmitting metasurface. Laser Photonics Rev. 2016, 10, 791-798.
- (27) Guo, T.; Argyropoulos, C. Broadband polarizers based on graphene metasurfaces. Opt. Lett. 2016, 41, 5592-5595.
- (28) Liu, X.; Fan, K.; Shadrivov, I. V.; Padilla, W. J. Experimental realization of a terahertz all-dielectric metasurface absorber. Opt. Express 2017, 25, 191-201.
- (29) Azad, A. K.; Kort-Kamp, W. J. M.; Sykora, M.; Weisse-Bernstein, N. R.; Luk, T. S.; Taylor, A. J.; Dalvit, D. A.; Chen, H. T. Metasurface broadband solar absorber. Sci. Rep. 2016, 6, 20347.

- (30) Meng, Y.; Hu, F.; Liu, Z.; Xie, P.; Shen, Y.; Xiao, Q.; Fu, X.; Bae, S.-H.; Gong, M. Chip-integrated metasurface for versatile and multiwavelength control of light couplings with independent phase and arbitrary polarization. *Opt. Express* **2019**, *27*, 16425–16439.
- (31) Meng, Y.; Liu, Z.; Xie, Z.; Wang, R.; Qi, T.; Hu, F.; Kim, H.; Xiao, Q.; Fu, X.; Wu, Q.; Bae, S.-H; Gong, M.; Yuan, X. Versatile on-chip light coupling and (de)multiplexing from arbitrary polarizations to controlled waveguide modes using an integrated dielectric metasurface. *Photonics Res.* **2018**, *8*, 564–576.
- (32) Guo, Y.; Pu, M.; Li, X.; Ma, X.; Song, S.; Zhao, Z.; Luo, X. Chip-integrated geometric metasurface as a novel platform for directional coupling and polarization sorting by spin-orbit interaction. *IEEE J. Sel. Top. Quantum Electron.* **2018**, 24, 4700107.
- (33) Zhang, Y.; Li, Z.; Liu, W.; Li, Z.; Cheng, H.; Chen, S.; Tian, J. Spin selective and wavelength selective demultiplexing based on waveguide integrated all dielectric metasurfaces. *Adv. Opt. Mater.* **2019**, *7*, 1801273.
- (34) Luo, W.; Xiao, S.; He, Q.; Sun, S.; Zhou, L. Photonic spin Hall effect with nearly 100% efficiency. *Adv. Opt. Mater.* **2015**, *3*, 1102–1108
- (35) Kang, M.; Feng, T. H.; Wang, H. T.; Li, J. S. Wave front engineering from an array of thin aperture antennas. *Opt. Express* **2012**, *20*, 15882–15890.
- (36) Yu, N.; Genevet, P.; Kats, M. A.; Aieta, F.; Tetienne, J.-P.; Capasso, F.; Gaburro, Z. Light propagation with phase discontinuities: generalized laws of reflection and refraction. *Science* **2011**, *334*, 333–337.
- (37) Zhou, Z.; Li, J.; Su, R.; Yao, B.; Fang, H.; Li, K.; Zhou, L.; Liu, J.; Stellinga, D.; Reardon, C. P.; Krauss, T. F.; Wang, X. Efficient silicon metasurfaces for visible light. *ACS Photonics* **2017**, *4*, 544.
- (38) Martins, A.; Li, J.; da Mota, A. F.; Wang, Y.; Neto, L. G.; do Carmo, J. P.; Teixeira, F. L.; Martins, E. R.; Borges, B. V. Highly efficient holograms based on c-Si metasurfaces in the visible range. *Opt. Express* **2018**, *26*, 9573–9583.
- (39) Guo, L. J. Nanoimprint lithography: methods and material requirements. *Adv. Mater.* **2007**, *19*, 495–513.
- (40) Zhang, C.; Subbaraman, H.; Li, Q.; Pan, Z.; Ok, J. G.; Ling, T.; Chung, C.-J.; Zhang, X.; Lin, X.; Chen, R. T.; Guo, L. J. Printed photonic elements: nanoimprinting and beyond. *J. Mater. Chem. C* **2016**, *4*, 5133–5153.